Published in final edited form as:
J Phys Chem C Nanomater Interfaces. 2009 November 12; 113(45): 19404–19410. doi:10.1021/jp906742q.

Luminescent Silica Core / Silver Shell Encapsulated with Eu(III) Complex

Jian Zhang, **Yi Fu**, and **Joseph R. Lakowicz***
Center for Fluorescence Spectroscopy, University of Maryland School of Medicine, Department of Biochemistry and Molecular Biology, 725 West Lombard Street, Baltimore, MD 21201

Abstract

In this paper we studied the metal-enhanced emission from long-lifetime lanthanide dyes that were encapsulated in the silver nanoshells. The metal nanoshells were synthesized with the silica spherical cores of 50 nm diameters and the silver shells of 5 – 60 nm. The optical properties of luminescent metal shells were performed on the either ensemble fluorescence spectroscopy or single particle imaging. The emission intensity from the encapsulated lanthanides was observed to enhance significantly by the metal nanoshell. The enhancement efficiency initially increased with the metal shell thickness and then decreased. The maximal enhancement occurred at the 20 – 30 nm thickness. The lifetime of encapsulated Eu(III) complexes was shorten dramatically indicating that they were coupled efficiently with the metal shells. The increased brightness and reduced lifetime of this core-shell structure demonstrate that the lanthanides are favorable for the single target molecule detections after encapsulating into the metal nanoshells.

Keywords

lanthanide; Eu(III) complex; silica sphere; silver nanoshell; metal enhanced fluorescence (MEF); plasmon resonance; near-field interaction; Radiative Decay Engineering (RDE)

Introduction

Lanthanides are known to display large Stokes shifts, narrow spectra, and long lifetimes [1, 2], which offer an opportunity to apply in an sensitive bioassay with a low detection background [3–6]. However, since the emission from the lanthanides involves an electron transition in a 4*f* orbital, which is forbidden, its absorbance coefficient is low and the emissive rate is slow that may lead to a low quantum yield and long decay time [7,8]. Consequently, we have to face several deficiencies. First, because of low quantum yield, the emission signal from the single lanthanide is too poor to be detectable in the single molecule detection (SMD). Second, although the lanthanide can be used as the probe to label the target molecule in the time-resolved *in vitro* studies of cell line or tissue to triggering the detection [8–10], the lifetime of ms scale is too long for the cellular autofluorescence. Additionally, a long decay time of lanthanide results in a low photon count rate, so that the lanthanide is bypassing undetectable at the single molecule level. To improve the optical properties of lanthanide in the time-resolved measurement and cell imaging, we developed a novel strategy that can increase the emission intensity and simultaneously shorten the lifetime in this research.

lakowicz@cfs.umbi.umd.edu.

Luminescent nanoparticles have been developed as the next generation of fluorophore and used widely in the clinical diagnostics and biological detections [11–14]. Lanthanides have been incorporated into the nanoparticle to increase the brightness [15–18]. Because of the large Stokes shifts [1,2], the fluorescence resonance energy transfer (FRET) cannot occur between the lanthanide molecules so the nanoparticle templates can be heavily loaded with the lanthanides to increase the emission signals. As a result, even though the quantum yields of lanthanides are not really enhanced, the emission signals from the lanthanide-encapsulated nanoparticles can be increased significantly. However, the lifetimes of encapsulated lanthanides are not shortened. In this paper, based on the metal enhanced fluorescence (MEF) principle, we developed a novel approach to further improve the emission intensity of lanthanide-contained nanoparticle and simultaneously shorten the lifetime by coating an external shell of silver. It is known that the emission intensity can be enhanced to $10 - 10^3$ folds by a near-field interaction of fluorophore with a local electric field induced by incident light when localizing a fluorophore near a metal nanoparticle with a subwavelength size [19–24]. The fluorophores can be bound onto the metal nanoparticles that are used as the luminescent nanoparticle probes in versatile strategies. In this research, we are particularly interested in the fluorophore-encapsulated core / metal-coated shell nanostructure because according to theoretical calculation, the interior electric field of metal shell is uniform and the fluorophore within the metal shell can be equally and efficiently coupled with the field [25–29]. In addition, the metal shell may also prevent entrance of oxygen and other species that react with the fluorophores and thus protect the fluorophores from the possible photochemical or other reactions. These characteristics have been demonstrated by our recent reports in which the metal-ligand complex $Ru(bpy)_3^{2+}$ and conventional organic fluorophore Rhodamine 6G were encapsulated into the silver nanoshells [30]. Although the lanthanides emit phosphorescent, somehow different from the fluorescence, according to a recent report from Geddes, we still anticipate that they can interact efficiently with the metal in the metal nanoshell and the optical properties can be improved [31]. Therefore, we synthesized the silica spheres with the Eu(III) complex encapsulation in this paper and then deposited the silver shells on the silica sphere templates to make the luminescent silica core/metal nanoshell structures. The optical properties of these luminescent nanoparticles were performed on the both ensemble spectroscopy and single particle emission imaging. Radiative Decay Engineering (RDE) theory was used to interpret the experiment results [34]. Although there are several publications on the interactions of lanthanides with the metal substrates [32,33], to our knowledge, it is the first report on a lanthanide-encapsulated core/metal shell structure.

Experimental Section

All reagents and spectroscopic grade solvents were used as received from Fisher or Sigma / Aldrich. Nanopure water (>18.0 MΩ cm^{-1}) purified using Millipore Milli-Q gradient system, was used in all experiments.

Synthesis of silica spheres with Eu(III) complex encapsulation

Monodispersed silica spheres were prepared using a modified Stöber method [35] and the Eu (III) complexes were physically absorbed in the silica spheres with the different contents during the silica sphere formation. Briefly, a serial amount of europium tris(3-(trifluoromethylhydroxy-methylene)-(+)-camphorate) (0.1 mg to 10 mg) were co-dissolved with tetraethyl orthosilicate (1.4×10^{-2} M) in 50 mL ethanol, respectively. 1.0 mL of 30% ammonia alcohol solution was added dropwise under vigorous stirring (Scheme 1). The solution became turbid after stirring overnight due to the formation of silica spheres. The mixture was centrifuged at 3000 rpm and the suspension was removed. The residuals were washed thoroughly with ethanol and then re-dispersed in 50 mL ethanol. Combining the washing solutions, the concentration of Eu(III) complex in solution could be estimated by the

emission measurements. The consumed amount of Eu(III) complex thus was estimated according to the concentration difference of after-reaction and before-reaction solution,. The consumed Eu(III) complexes were regarded to encapsulate in the silica spheres. The re-dispersed spheres were thiolated by adding 10 μL 3-thiolpropyltrimethoxy silane and stirring for 12 h. Centrifuged at 3,000 rpm, washed with ethanol, and redispersed in 10 mL water, the concentration of silica sphere was estimated to be 6×10^{-8} M in solution if the loss was neglected in the treatments.

Deposition of metal nanoshell

The small silver colloids were conjugated to the silica spheres as the seeds for the metal shell growths. By reduction of silver precursor, the silver shells were grown on the metal-seeded silica spheres layer-by-layer [30]. The small seeded silver colloids (*average* diameter = 5 nm) were prepared by chemical reduction of silver nitrate using ascorbic acid [36]. Briefly, 10 mg of silver nitrate and 30 mg of trisodium citrate were co-dissolved in 50 mL of water. 1 mL of 0.1 N NaOH aqueous solution was added under stirring for 2 min, and then 20 mg of ascorbic acid in 10 mL water was added dropwise for 5 min. The reaction solution was stirring for additional 1 h and became yellow color. 10 mL of silica sphere suspension and 50 mL of silver colloidal solution were co-dissolved with continuous stirring for 2 h. The supernatant was removed by centrifugation at 3,000 rpm and the precipitate was washed with water. The solid residues were grey color significantly different from the untreated white silica spheres, indicating that the silver colloids had been conjugated on silica spheres. The residues were redispersed in 10 mL water. The silver shells were grown on the silver-seeded silica spheres by chemical reduction of 1 mL of $Ag(NH_3)^{2+}$ (10 mM) by 1 mL of glucose (20 mM) water solution. The reaction solution was stirred for 3 h at room temperature. Washed with water and recovered by centrifugation, the formed silver shells were redissolved in water and treated repetitively to grow the silver shell layer-by-layer. The amount of silver precursor was adjusted in each operation to control the increase of silver thickness on the silica spheres as the cores. During the metal shell growths on the silica templates, the silver precursors have to be reduced under mild conditions. Otherwise, many metal spherical nanoparticles will be found on the TEM images. In this research, we noticed that if there was no metal-seeded silica sphere added in solution, the reduction to the silver precursors could not occur significantly indicating that the reduced silver was deposited principally on the silica spheres as the shell structures.

Spectra and TEM measurements

Absorption spectra were monitored with a Hewlett Packard 8453 spectrophotometer. Fluorescence spectra and lifetimes were recorded with a Cary Eclipse Fluorescence Spectrophotometer. After excitation, the emission was acquired by a gate pulse widths of 0.5 ms. Delay time and decay time were adjusted to 0.1 ms and 5 ms, respectively.

For the fluorescence imaging measurements, the glass coverslips were first soaked in a 10:1 (v:v) mixture of concentrated H_2SO_4 and 30% H_2O_2 overnight, extensively rinsed with water, sonicated in absolute ethanol for 2 min and dried with air stream. A dilute solution was dispersed on the pre-cleaned coverslip. All measurements were performed using a time-resolved confocal microscopy (MicroTime 200, PicoQuant). Briefly, it consists of an inverted microscope coupled to a high-sensitivity detection setup. A single-mode pulsed laser diode was used as the excitation source. An oil immersion objective (Olympus, 100×, 1.3NA) was employed both for focusing laser light onto the samples and collecting fluorescence emission from the samples. The fluorescence that passed a dichroic mirror was focused onto a 75 μm pinhole for spatial filtering to reject out-of-focus signals. The integration time was 0.6 ms per pixel. The data was stored in the time-tagged-time-resolved (TTTR) mode that allowed recording every photon with its individual timing information with regard to both the location or sample and time delay between the excitation and emission.

Transmission electron micrographs (TEM) were taken with a side-entry Philips electron microscope at 120 keV. Samples were cast from water solutions onto standard carbon-coated (200–300 Å) Formvar films on copper grids (200 mesh) by placing a droplet of a diluted aqueous sample solution on grids. The size distribution of the metal cores was analyzed with Scion Image Beta Release 2 counting at least 200 particles.

Results and Discussion

In this research, the silica spheres with the Eu(III) complex encapsulation were synthesized in a modified Stöber method [35]. From the TEM images, these silica spheres were approximately homogeneous in the size distribution and the average diameter was about 50 nm (Figure 1). In the formation reaction, 0.1 – 10 mg Eu(III) complex was dissolved in solution to absorb in the silica spheres. The contents of Eu(III) complex absorbed in the silica spheres were found to depend on the complex concentration in the reaction solution. It was noticed that the absorption was strong in the silica matrix and no significant Eu(III) complex was leaked during storage and chemical modification. Over 10 mg Eu(III) complex in solution could lead to the overloading of complex in the silica spheres and the absorbed complexes began to leak into aqueous solution. The content of Eu(III) complex in the formed silica sphere could be estimated from the consumed complex amount in the reaction before and after the reaction, which was in a range of $1 \times 10^{-4} – 1 \times 10^{-2}$ M, increasing with an increase of complex concentration in the reaction solution. Considering that the diameter of silica sphere was 50 nm, the number of Eu(III) complex was inferred in a range of 3 – 300 lanthanide molecule / silica sphere.

The silica core / metal shell structures were generated by depositing the metal nanoshells on the silica spheres with the Eu(III) complex encapsulation. Typically, the silica spheres were first thiolated by surface silane reaction and then the small silver colloids were conjugated on the sphere surfaces to work as the seeds for the smooth growths of metal shells [25]. On these seeded silica sphere templates, the silver shells were deposited layer-by-layer by the reduction of silver salt from solution. The TEM images can verify the growths of metal shells on the silica spheres (Figure 1). The shell thickness was determined by two alternative strategies. First is the consumed amount of silver precursor in the reaction. The second is the apparent diameter of nanoparticle on the TEM images. We noticed that the measured shell thickness on the TEM images was about 1.5 times greater than the estimated value from the consumed amount of silver precursor. The reason is the porosity of formed metal shells. Actually, the margins of metal nanoshells were observed to be rough. We strictly controlled the amount of silver precursor in each repetitive treatment, so the silver accumulation on the silica sphere could lead to an approx. 10 nm increase of metal thickness besides the first layer was about 5 nm. The thickness of metal nanoshell is an important factor to tune the optical properties and control the interaction with the encapsulated fluorophores to induce the fluorescence enhancement. Because the size of metal nanoshells does not seem quite homogeneous from the TEM images, we presented the statistical distribution (down panel in Figure 1). Since the optical properties were mostly performed on the ensemble spectra, so we cannot isolate the contribution of mono-dispersed nanoshell. But the relation between the statistically estimated metal thickness of nanoshell and estimated optical properties can imply the dependence of fluorescence enhancement on the metal shell thickness in this case.

Because of strong light scattering, the synthesized silica sphere did not express a well-defined absorption spectrum (Figure 2). On the other hand, with the metal accumulation on the silica sphere surface, the metal plasmon resonance appeared at 400 nm and became intensive and broaden, consistent with the previous observations [25,30]. Upon excitation at 330 nm, the Eu (III)-encapsulated silica sphere in the absence of metal exhibited an emission spectrum with the maximum at 616 nm, 6 nm red shifting from the free Eu(III) complex (Figure 3). In addition, we noticed that the emission band from the encapsulated complex was broadened significantly,

which was due to the restriction to the movement of complex in the solid template [37]. No significant shift of emission maximum was observed even though the silica sphere was heavily loaded with 300 lanthanides / silica sphere, indicating the complexes were encapsulated as the monomers without the aggregation. The absence of interaction between the Eu(III) complexes in the silica matrix was further indicated by the observation that the emission intensity at 616 nm was proportionally increased with the content of Eu(III) complex in the silica sphere without a down-deviation (Figure 4). The similar situation was also observed for the metal nanoshells, which was due to the large Stokes shifts of lanthanides. Therefore, the luminescent metal nanoshells were prepared with the high loading of Eu(III) complex in the silica cores for the investigation of their optical properties in this case.

The metal nanoshells with the Eu(III) encapsulation displayed an emission maximum at 616 nm, showing an insignificant shift from the silica spheres in the absence of metal (Figure 3). However, the emission intensity from the encapsulated lanthanides was observed to enhance significantly on the either ensemble spectrum at the same concentration or single particle imaging measurement. All experimental results obtained by different strategies were employed to estimate the enhancement efficiency by the metal nanoshells. For the ensemble measurements, the enhancement efficiency was estimated by the ratio of emission intensity of metal shell over silica sphere in the absence of metal at the same concentration in solution. NaCN was used to remove the metal shells and release the silica spheres as free into solution. In the treatment, it was observed that accompanying with the dissolution of metal shell by NaCN, the emission intensity was decreased progressively with the reaction time, corresponding to the loss of enhancement effect by the metal shell. The concentration of released silica sphere in solution that could be estimated quantitatively from the emission intensity [11] was regarded to be the same as that of metal nanoshell. Therefore, the enhancement efficiency by the metal shell was estimated. We also normalized the emission spectra of metal shells with the various metal thicknesses to the same concentration to investigate the metal thickness-dependent enhancement (Figure 5). It was observed that the emission intensity of these metal shells increased with the metal thickness at initial, reached to saturation at 20 – 30 nm, and then decreased. The estimated enhancement efficiency was plotted against the metal thickness (Figure 6), showing the saturation of 9-fold at 20 nm silver thickness. The enhancement efficiency for the silver shells with the different Eu(III) complex loading in the silica cores exhibited the close maximal enhancement efficiency at the 20 nm metal thickness, independence of the content, indicating that the interaction between the encapsulated Eu(III) complexes could be negligible in these silver shells.

The imaging measurements were performed on laser scanning confocal microscopy. Because the solution was diluted to the nano mole scale in the cast, the most collected images were believed to come from the single luminescent shells. The encapsulated Eu(III) complexes had to be excited by a laser diode of 470 nm because of an absence of UV laser source. No emission signals could be collected for the free Eu(III) complexes and only very dim emission signals were observed from the Eu(III) encapsulated silica spheres in the absence of metal. Considering the low quantum yield of lanthanides, the results are reasonable. For the silver shells, the images were totally different. It was noticed that the emission signals from the isolated luminescent metal nanoshells were strong and the emission intensities were enhanced with an increase of metal thickness. Compared with the emission intensity of silica sphere in the absence of metal, the enhancement efficiencies of metal shells were estimated and plotted against the metal thickness (Figure 6), showing a curve close to the ensemble measurement. The maximal efficiency was 11, close to that from the ensemble measurement. The small difference could come from the measurement conditions: the imaging under dry condition but the ensemble in wet solution.

The metal enhanced fluorescence (MEF) is considered to occur via a near-field interaction when localizing a fluorophore on a metal surface. According to the RDE theory, the fluorescence enhancement is accomplished through an increase of intrinsic decay rate of fluorophore. The mechanism is complicated and we can only offer a simply discussion herein. It is known that for a free-space emission of an excited fluorophore, the quantum yield (Q_o) and lifetime (τ_o) can be expressed as eqs. 1 and 2,

$$Q_o=\Gamma/(\Gamma+k_{nr}) \tag{1}$$

$$\tau_o=(\Gamma+k_{nr})^{-1} \tag{2}$$

A fluorophore can be regarded as a dipole to be in the proximity and interact with a metal particle [34]. Suppose the radiative decay rate near the metal is increased and is given by $\Gamma + \Gamma_m$, when Γ_m is the additional rate due to the metal substrate, the quantum yield Q_m and lifetime τ_m of the fluorophore near the metal substrate thus become

$$Q_m=\frac{\Gamma+\Gamma_m}{\Gamma+\Gamma_m+k_{nr}} \tag{3}$$

$$\tau_m=(\Gamma+\Gamma_m+k_{nr})^{-1} \tag{4}$$

As a result, the metal-induced change to $\Gamma + \Gamma_m$ can cause an increase of quantum yield and a decrease of lifetime. Thus, the radiate rate by metal substrate (Γ_m) is regarded to play an important role in the fluorescence enhancement. Because the interior electric field is calculated to be uniform in the metal shell, the fluorophore within the metal shell can be equally and efficiently coupled with the local field and the emission intensity by the luminescent metal shell can be enhanced. The decrease of radiative rate can be reflected by a clear change of lifetime [34]. The lifetimes were measured on the ensemble spectra. The collected emission decay curves were analyzed in terms of a sum of individual single exponential decays [14a]:

$$I(t)=\sum_{i=1}^{n}\alpha_i\exp(-t/\tau_i) \tag{5}$$

In this expression τ_i are the decay times and α_i are the amplitudes. The fractional contribution of each component to the steady-state intensity is described by:

$$f_i=\frac{\alpha_i\tau_i}{\sum_j\alpha_j\tau_j} \tag{6}$$

The average lifetime is represented by:

$$\overline{\tau} = \sum_i f_i \tau_i \quad (7)$$

The decay curves of the free Eu(III) complex, encapsulated in the silica sphere in the absence of metal, and encapsulated in the silver shell were shown in the inset of Figure 8 expressing the significant differences. The estimated parameters were listed in Table 1. The average lifetime of free Eu(III) complex in solution was 75 μs close to the literature report. Although some χ_R^2 values are above 1.3 in the analysis, the most measured lifetime values are reliable to the discussion of experimental results. The average lifetime of Eu(III) complex in the silica sphere is estimated to be 137 μs, longer than the free complex, which is attributed to the movement restriction to the complex in the silica template. Relative to the silica sphere in the absence of metal, the silver nanoshells exhibited the dramatically shortened lifetimes. The average lifetime was plotted against the metal thickness (Figure 8), showing an initial decrease. We also noticed that the decrease of average lifetime was precisely contrary to the intensity enhancement with the metal thickness (Figure 6), revealing that the both changes of emission intensity and lifetime were due to the coupling interactions with the metal shells and the interactions were strengthened with an increase of metal thickness. The lifetime was shortened to 8.7 μs at the 20 nm metal shell, only 6% of the average lifetime value to the silica sphere in the absence metal. This decrease percentage of lifetime is even greater than the increase percentage of intensity indicating that the increase of intrinsic decay rate takes a key role in the MEF-related characteristics for the Eu(III)-encapsulated metal shells.

We also tried to interpret the experiment results with the metal thickness-dependence. This effect depends on different physical and chemical parameters, and the mechanism is believed to be complicated. There are huge amount of reports and some of them are even contradictory. Thus, we cannot find an exact approach to explain the experiment results in this case. However, it is clear that because the fluorophore is not altered significantly in the system, the interior electric field within the metal nanoshell is important to enhance the emission from the encapsulated (Eu(III) complexes. According Halas et al, the incident white light is scattered by the nanoshells and couples to the surface plasmon mode [38]. The calculation to the interior electric field from their model reveals that the inner electric field density is proportional to $(r_1/ r_2)^6$, in which r_1 and r_2 represent the inner and outer radius, respectively, for the metal nanoshell. In the case, the inner radius of silica core is not altered but the outer radius is increased with an increase of metal thickness indicating that the interior electric field density may reduce with an increase of metal thickness. A similar result is also reported by El-Sayed, et al, who claim that the plasmon sensitivity of gold or silver nanoshell falls near-exponentially as a function of the shell thickness ($r_2 - r_1$)-to-core radius (r_1) ratio with a constant of 0.2 [39, 40]. In this case, the silica core is 50 nm, so the maximal enhancement is expected to occur at 5 nm thick metal shell, thinner than our experimental result. The reason is that there are many defects on the metal thin shells and these defects can reduce the field density within the metal shell. In addition, the differences on the experiment and theory are due to the different effects of far- and near-fields on the metal nanoshells when the fluorescence emits through the metal nanoshells to far field. In this case only near-field interaction is considered but the far field is ignored. Thus we cannot claim that this treatment is complete and definitive. However, this discussion can offer us a glimpse into the nature of metal-fluorophore interactions, i.e. an increase of interior near-field in the metal shell can lead to an increase of fluorescence emission from fluorophores within a local electric field.

Conclusions

Lanthanides have been used in the time-resolved assays because of their long lifetimes and narrow emission bands that can result in low emission backgrounds. However, the weak emission signals of them also limit the applications. To improve the optical properties of these lanthanides, in this research, we developed a novel silica core/metal shell structure to encapsulate the lanthanides in the silica spheres and then built the silver nanoshells outsides. These luminescent metal nanoshells were studied using either the ensemble spectrum or single particle imaging method. The results revealed that the emission intensity of encapsulated Eu (III) complex was significantly enhanced with an increase of the metal thickness at initial period accompanying with a dramatic decrease of lifetime. The maximal enhancement efficiency was about 10. Compared with the single Eu(III) complex, the single metal shell was even 2,000-fold brighter, which was estimated based on the ensemble spectral measurements when the free Eu(III) complex and metal nanoshell were dissolved at the same concentration in solution. Thus, such increase of brightness includes the effects from both multiple fluorophores and metal enhancement. These lanthanide-encapsulated metal shells can be detected at the single particle level in the imaging measurements. With the silica core of 50 nm and metal shell of 20 nm, the luminescent metal shell has a total diameter smaller than 100 nm. Thus, they are expected to enable immuno-interact with the targets on the cell surfaces or even permeate through the cell membrane and conjugate with the targets in the cells. The lifetimes of encapsulated lanthanides in the metal shell remain to be much longer than the cellular autofluorescence, so they may offer a considerable promise in a time-resolved *in vitro* diagnostics with strong emission signals but low emission backgrounds.

Acknowledgments

This research was supported by grants from NIH (JZ: EB009509 and JR: HG-00255, EB006521, EB00682).

References

1. (a) Richardson FS. Chem Rev 1982:541. (b) Riehl JP, Richardson FS. Chem Rev 1986;86:1.
2. (a) Parker D, Dickins RS, Puschmann H, Crossland C, Howard JAK. Chem Rev 2002;102:1977. [PubMed: 12059260] (b) Tsukube H, Shinoda S. Chem Rev 2002;102:2389. [PubMed: 12059273]
3. Moore EG, Xu J, Jocher CJ, Werner EJ, Raymond KN. J Am Chem Soc 2006;128:10648. [PubMed: 16910637]
4. Karşilayan H, Hemmilä I, Takalo H, Toivonen A, Pettersson K, Lövgren T, Mukkala VM. Bioconjugate Chem 1997;8:71.
5. Takalo H, Mukkala VM, Mikola H, Liitti P, Hemmila I. Bioconjugate Chem 1994;5:278.
6. Nishioka T, Yuan J, Yamamoto Y, Sumitomo K, Wang Z, Hashino K, Hosoya C, Ikawa K, Wang G, Matsumoto K. Inorg Chem 2006;45:4088. [PubMed: 16676970]
7. Terai T, Kikuchi K, Iwasawa S, Kawabe T, Hirata Y, Urano Y, Nagano T. J Am Chem Soc 2006;128:6938. [PubMed: 16719474]
8. Yuan J, Wang G, Majima K, Matsumoto K. Anal Chem 2001;73:1869. [PubMed: 11338604]
9. Vancaeyzeele C, Ornatsky O, Baranov V, Shen L, Abdelrahman A, Winnik MA. J Am Chem Soc 2007;129:13653. [PubMed: 17929920]
10. Tan M, Ye Z, Wang G, Yuan J. Chem Mater 2004;16:2494.
11. Rosi NL, Mirkin CA. Chem Rev 2005;105:1547. [PubMed: 15826019]
12. LaFratta CN, Walt DR. Chem Rev 2008;108:614. [PubMed: 18229955]
13. Thomas KG, Kamat PV. Acc Chem Res 2003;36:888. [PubMed: 14674780]
14. (a) Lakowicz, JR. Principles of Fluorescence Spectroscopy. 3. Springer Published; New York: 2006. (b) Lakowicz, JR. Emerging biomedical application of time-resolved florescence spectroscopy, Topic in Fluorescence spectroscopy. In: Lakowicz, JR., editor. Probe Design and Chemical Sensing. Vol. 4. Plenum Press; New York: 1994.

15. (a) Peng H, Wu C, Jiang Y, Huang S, McNeill J. Langmuir 2007;23:1591. [PubMed: 17279632] (b) Peng C, Zhang H, Yu J, Meng Q, Fu L, Li H, Sun L, Guo X. J Phys Chem B 2005;109:15278. [PubMed: 16852935] (c) DeOliveira E, Neri CR, Serra OA, Prado AGS. Chem Mater 2007;19:5437.
16. (a) Gago S, Fernandes JA, Rainho JP, Sá Ferreira RA, Pillinger M, Valente AA, Santos TM, Carlos LD, Ribeiro-Claro PJA, Gonçalves IS. Chem Mater 2005;17:5077. (b) Wang H, Yu M, Lin C, Liu X, Lin J. J Phys Chem C 2007;111:11223. (b) Lin C, Kong D, Liu X, Wang H, Yu M, Lin J. Inorg Chem 2007;46:2674. [PubMed: 17338518] (c) Ye Z, Tan M, Wang G, Yuan J. Anal Chem 2004;76:513. [PubMed: 14750841] (d) Guo X, Guo H, Fu L, Deng R, Chen W, Feng J, Dang S, Zhang H. J Phys Chem C 2009;113:2603.
17. (a) Soares-Santos PCR, Nogueira HIS, Félix V, Drew MGB, Ferreira RAS, Carlos LD, Trindade T. Chem Mater 2003;15:100. (b) Liu JL, Yan B. J Phys Chem B 2008;112:10898. [PubMed: 18698700] (c) Cousinié S, Gressier M, Reber C, Dexpert-Ghys J, Menu MJ. Langmuir 2008;24:6208. [PubMed: 18489189]
18. (a) Tang S, Zhao J, Storhoff JJ, Norris PJ, Little RF, Yarchoan R, Stramer SL, Patno T, Domanus M, Dhar A, Mirkin CA, Hewlett IK. J Acquir Immune Defic Syndr 2007;46:231. [PubMed: 17693896] (b) Oyewumi MO, Mumper RJ. Bioconjugate Chem 2002;13:1328. (c) Chen Y, Chi Y, Wen H, Lu Z. Anal Chem 2007;79:960. [PubMed: 17263322] (d) Zhang H, Xu Y, Yang W, Li Q. Chem Mater 2007;19:5875.
19. Sokolov K, Chumanov G, Cotton TM. Anal Chem 1998;70:3898. [PubMed: 9751028]
20. (a) Yu F, Persson B, Lofas S, Knoll W. J Am Chem Soc 2004;126:8902. [PubMed: 15264814] (b) Ekgasit S, Thammacharoen C, Yu F, Knoll W. Anal Chem 2004;76:2210. [PubMed: 15080730] (c) Baluschev S, Yu F, Miteva T, Ahl S, Yasuda A, Nelles G, Knoll W, Wegner G. Nano Lett 2005;5:2482. [PubMed: 16351199]
21. (a) Stoermer RL, Keating CD. J Am Chem Soc 2006;128:13243. [PubMed: 17017805] (b) Xie F, Baker MS, Goldys EM. Chem Mater 2008;20:1788. (c) Xie F, Baker MS, Goldys EM. J Phys Chem B 2006;110:23085. [PubMed: 17107148]
22. (a) Sherry LJ, Chang SH, Schatz GC, Van Duyne RP, Wiley BJ, Xia Y. Nano Lett 2005;5:2034. [PubMed: 16218733] (b) Oubre C, Nordlander P. J Phys Chem B 2005;109:10042. [PubMed: 16852215]
23. van Dijk MA, Lippitz M, Orrit M. Acc Chem Res 2005;38:594. [PubMed: 16028894]
24. (a) Hubert C, Rumyantseva A, Lerondel G, Grand J, Kostcheev S, Billot L, Vial A, Bachelot R, Royer P, Chang S-h, Gray SK, Wiederrecht GP, Schatz GC. Nano Lett 2005;5:615. [PubMed: 15826096] (b) Payne EK, Shuford KL, Park S, Schatz GC, Mirkin CA. J Phys Chem B 2002;106:2150.
25. (a) Wang H, Goodrich GP, Tam F, Oubre C, Nordlander P, Halas NJ. J Phys Chem B 2005;109:11083. [PubMed: 16852350] (b) Nehl CL, Grady NK, Goodrich GP, Tam F, Halas NJ, Hafner JH. Nano Lett 2004;4:2355. (c) Jackson JB, Halas NJ. J Phys Chem B 2001;105:2743. (d) Pham T, Jackson JB, Halas NJ, Lee TR. Langmuir 2002;18:4915. (e) Hirsch LR, Jackson JB, Lee A, Halas NJ, West JL. Anal Chem 2003;75:2377. [PubMed: 12918980]
26. (a) Olson TY, Schwartzberg AM, Orme CA, Talley CE, O'Connell B, Zhang JZ. J Phys Chem C 2008;112:6319. (b) Neretina S, Qian W, Dreaden E, El-Sayed MA, Hughes RA, Preston JS, Mascher P. Nano Lett 2008;8:2410. [PubMed: 18578550]
27. (a) Wang Y, Xie X, Wang X, Ku G, Gill KL, O'Neal DP, Stoica G, Wang LV. Nano Lett 2004;4:1689. (b) Alvarez-Puebla RA, Ross DJ, Nazri GA, Aroca RF. Langmuir 2005;21:10504. [PubMed: 16262313]
28. (a) Enderlein J. Phys Chem Chem Phys 2004;4:2780. (b) Enderlein J. Appl Phys Letter 2002;80:315.
29. (a) Hao E, Li S, Bailey RC, Zou S, Schatz GC, Hupp JT. J Phys Chem B 2004;108:1224. (b) Tanabe K. J Phys Chem C 2008;112:15721.
30. (a) Zhang J, Fu Y, Lakowicz JR. J Phys Chem C 2007;111:1955. (b) Zhang J, Gryczynski I, Gryczynski Z, Lakowicz JR. J Phys Chem B 2006;110:8986. [PubMed: 16671705]
31. Zhang Y, Aslan K, Previte MJR, Geddes CD. Appl Phys Lett 2008;92:013905.
32. Selvan ST, Hayakawa T, Nogami M. J Phys Chem B 1999;103:7064–7067.
33. Wu M, Lakowicz JR, Geddes CD. J Fluro 2005;15:53.
34. (a) Lakowicz JR. Anal Biochem 2001;298:1. [PubMed: 11673890] (b) Lakowicz JR. Anal Biochem 2005;337:171. [PubMed: 15691498]

35. Stöber W, Fink A, Bohn E. J Colloid Interface Sci 1968;26:62.
36. Zhang J, Fu Y, Chowdhury M, Lakowicz JR. J Phys Chem C 2008;112:18.
37. Hu J, Zhang J, Liu F, Kittredge K, Whitesell JK, Fox MA. J Am Chem Soc 2001;123:1464.
38. Prodan E, Nordlander P, Halas N. J Nano Lett 2003;3:1411. (b) Fofang NT, Park TH, Neumann O, Mirin NA, Nordlander P, Halas N. J Nano Lett 2008;8:3481.
39. Jain PK, Huang X, El-Sayed IH, El-Sayed MA. Acc Chem Res 2008;41:1578. [PubMed: 18447366]
40. Jain PK, El-Sayed MA. J Phys Chem C 2007;111:17451.

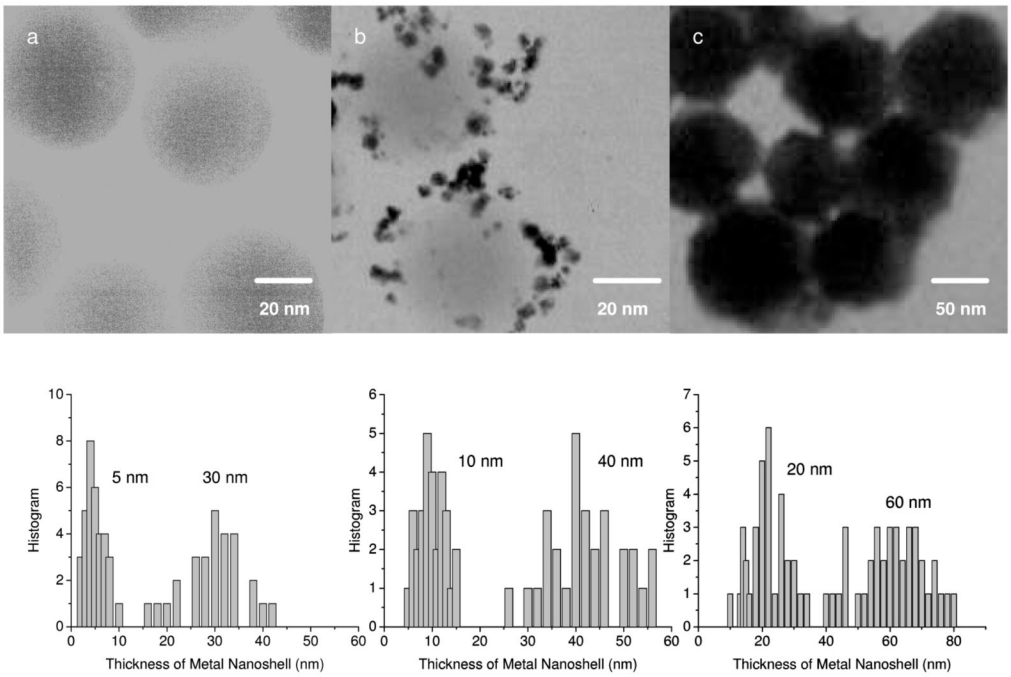

Figure 1.

Upper panel: TEM images of (a) silica spheres, (b) silver-seeded silica spheres, and (c) 30 nm thick silver nanoshells. Bottom panel: statistical distributions of metal shell thickness that were estimated by the substation of silica sphere radius (25 nm) from the metal particle radius on the TEM images. At lease 20 metal nanoparticle images were treated for each sample.

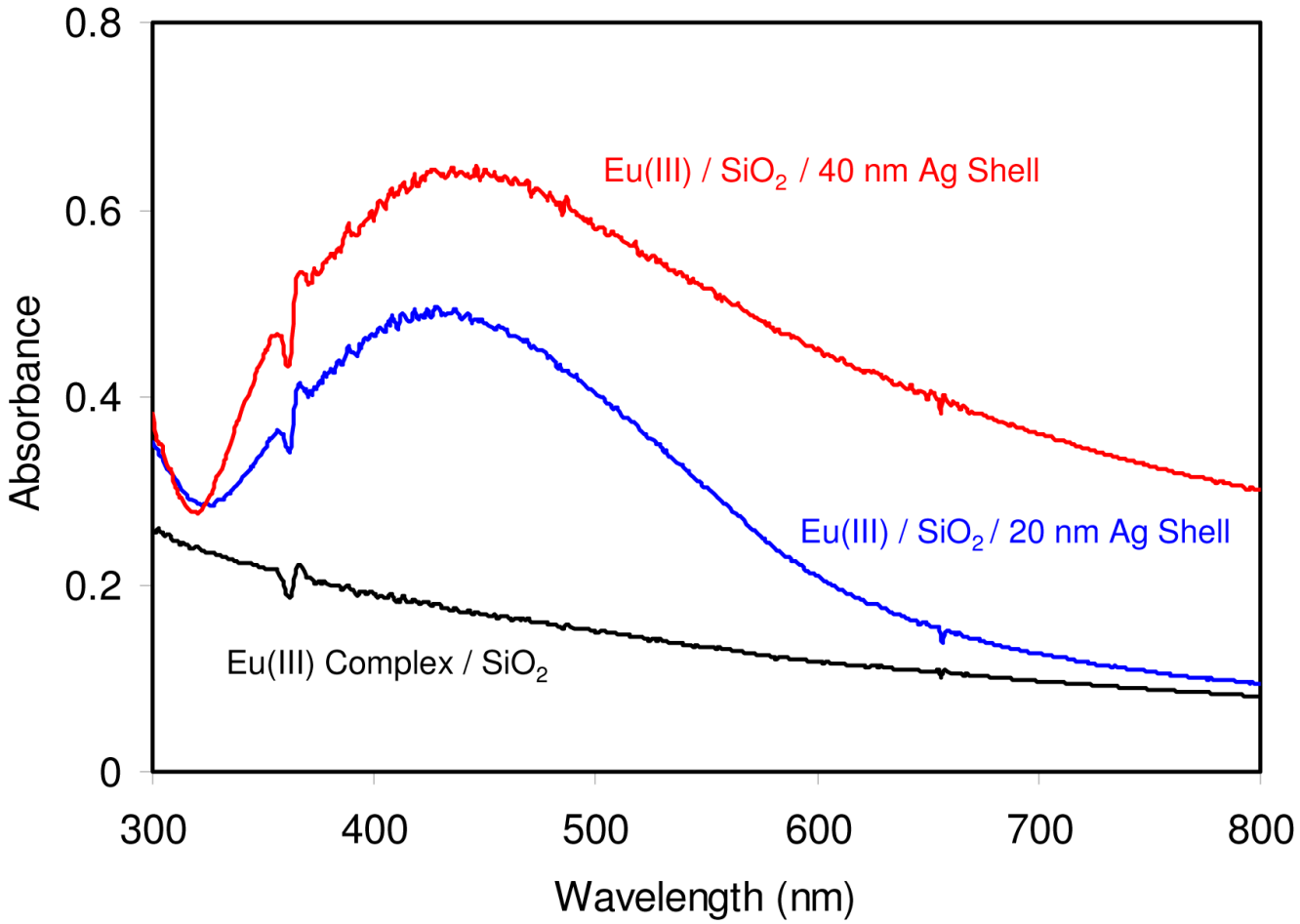

Figure 2.
Absorbance spectra of Eu(III)-encapsulated silica spheres, 20 nm thick Eu(III)-encapsulated silica / silver nanoshells, and 40 nm thick Eu(III)-encapsulated silica / silver nanoshells in water.

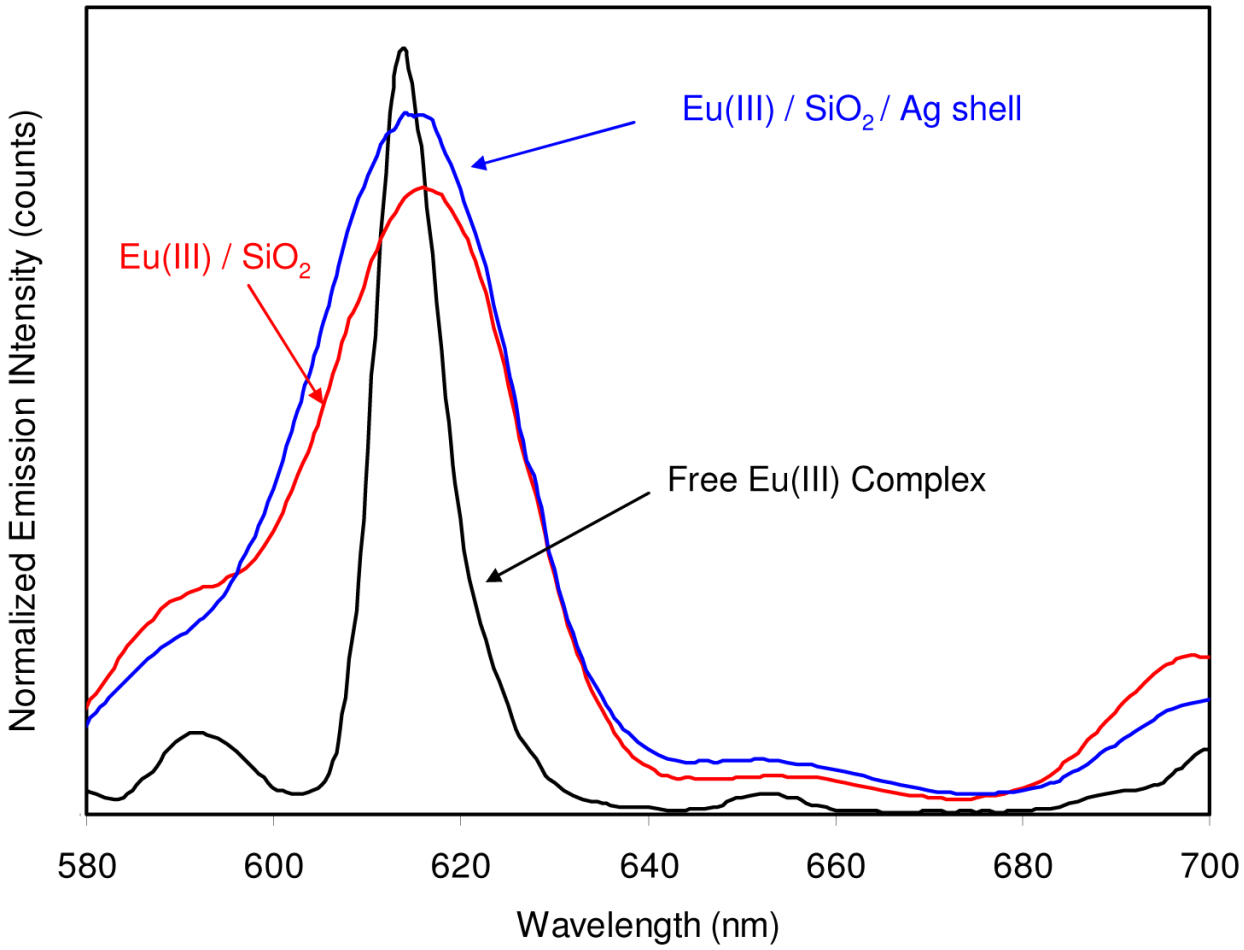

Figure 3.
Emission spectra of free Eu(III) complex, Eu(III)-encapsulated silica spheres, and Eu(III)-encapsulated silica / silver nanoshells upon excitation at 330 nm. The concentrations of silica sphere and silver sphere remain to be 1×10^{-4} M in solution for all samples.

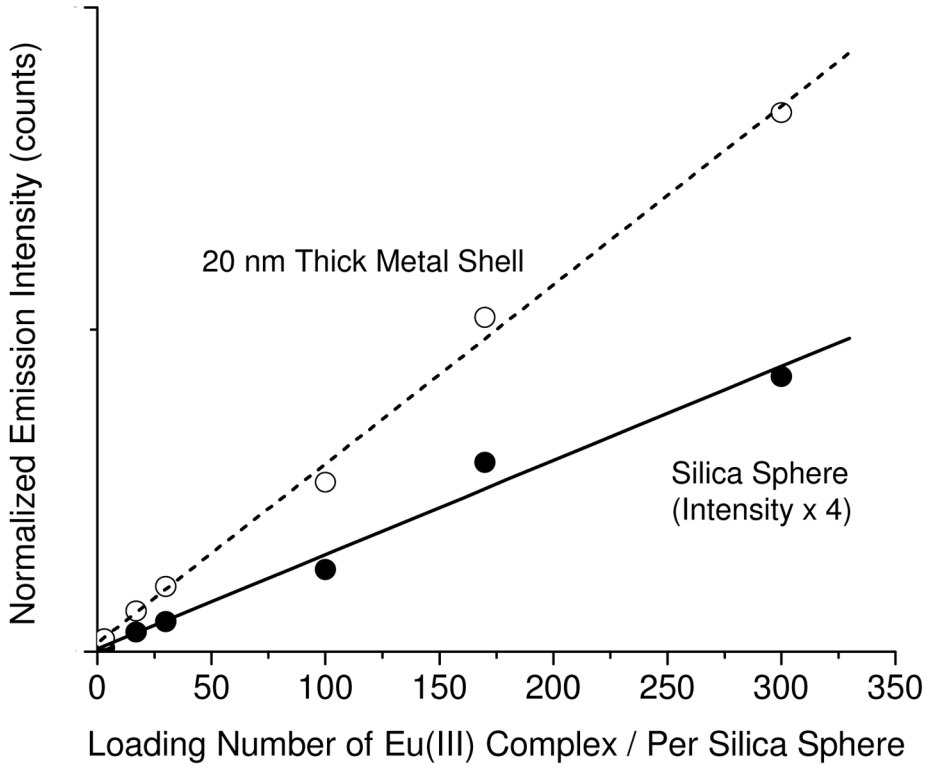

Figure 4.
Dependences of the emission intensities of Eu(III)-encapsulated silica spheres and Eu(III)-encapsulated silica core/silver shell structures on the Eu(III) concentrations in the silica cores. The metal thickness was 20 nm for this sample.

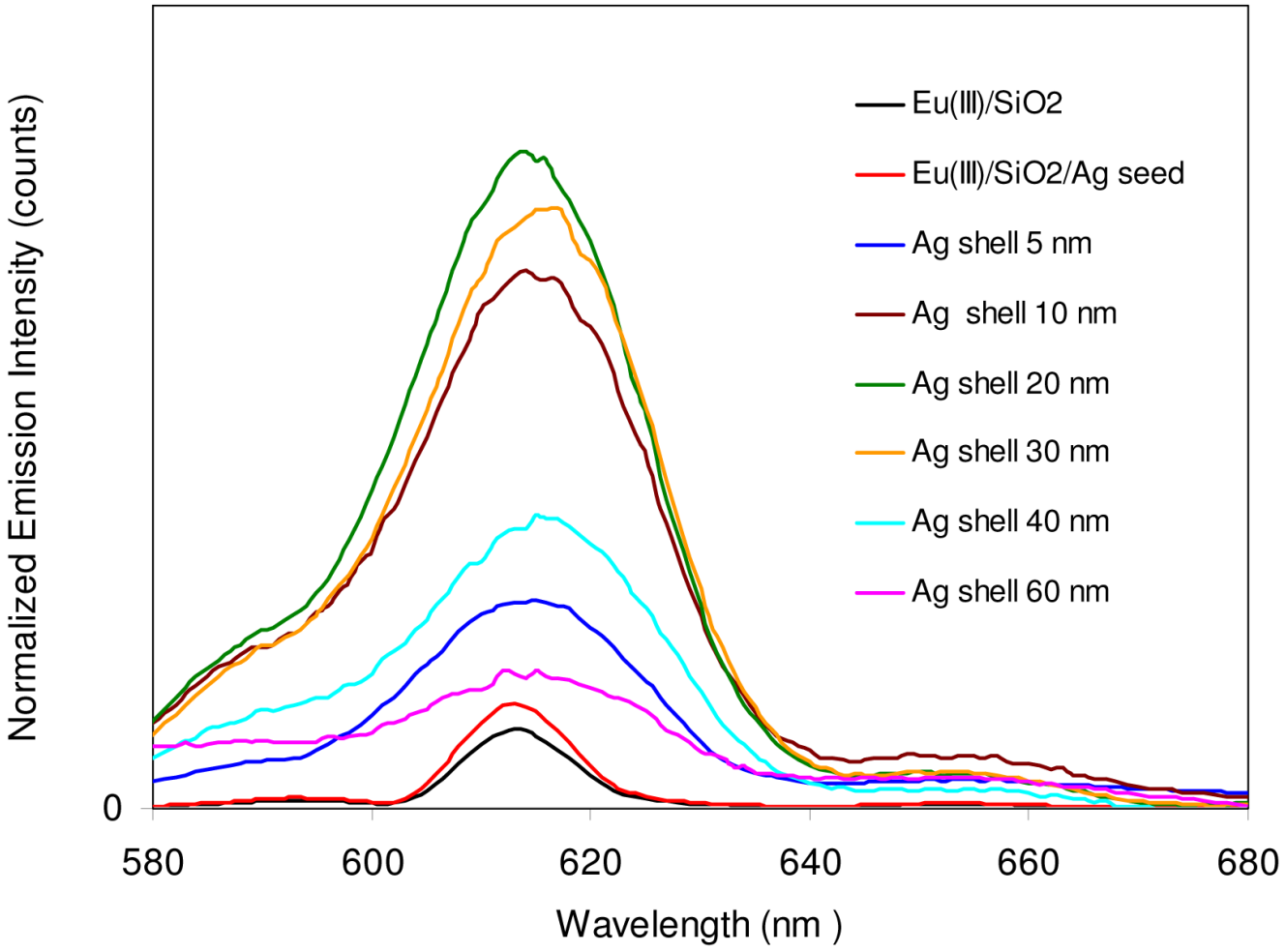

Figure 5.
Normalized emission spectra of Eu(III)-encapsulated silica/silver shell structures with the same complex concentration of 1×10^{-4} M in the 50 nm silica cores but different thick metal shells from 0 – 60 nm.

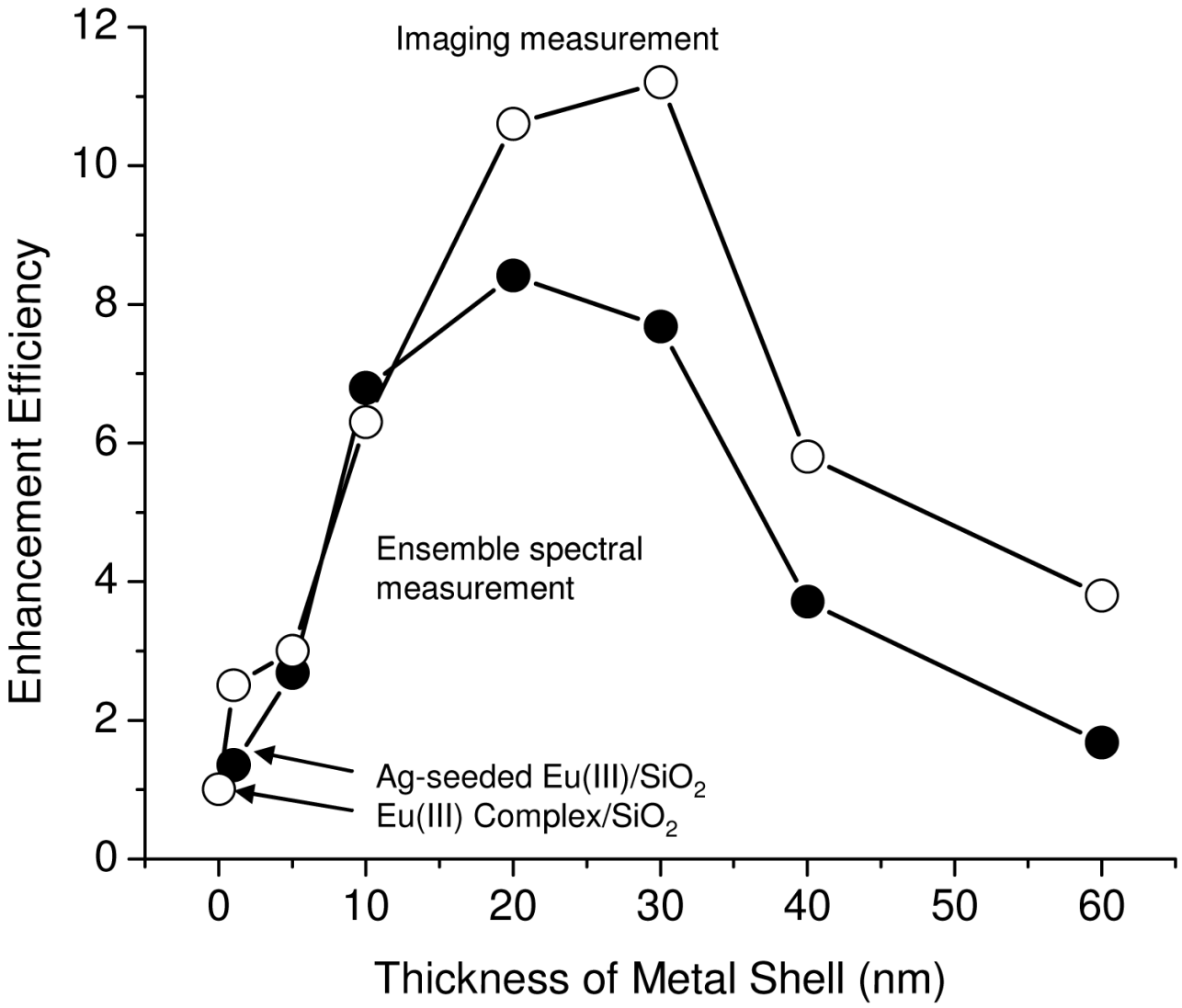

Figure 6.
Dependences of the enhancement efficiency on the metal shell thickness achieved by the either ensemble spectrum or single particle imaging.

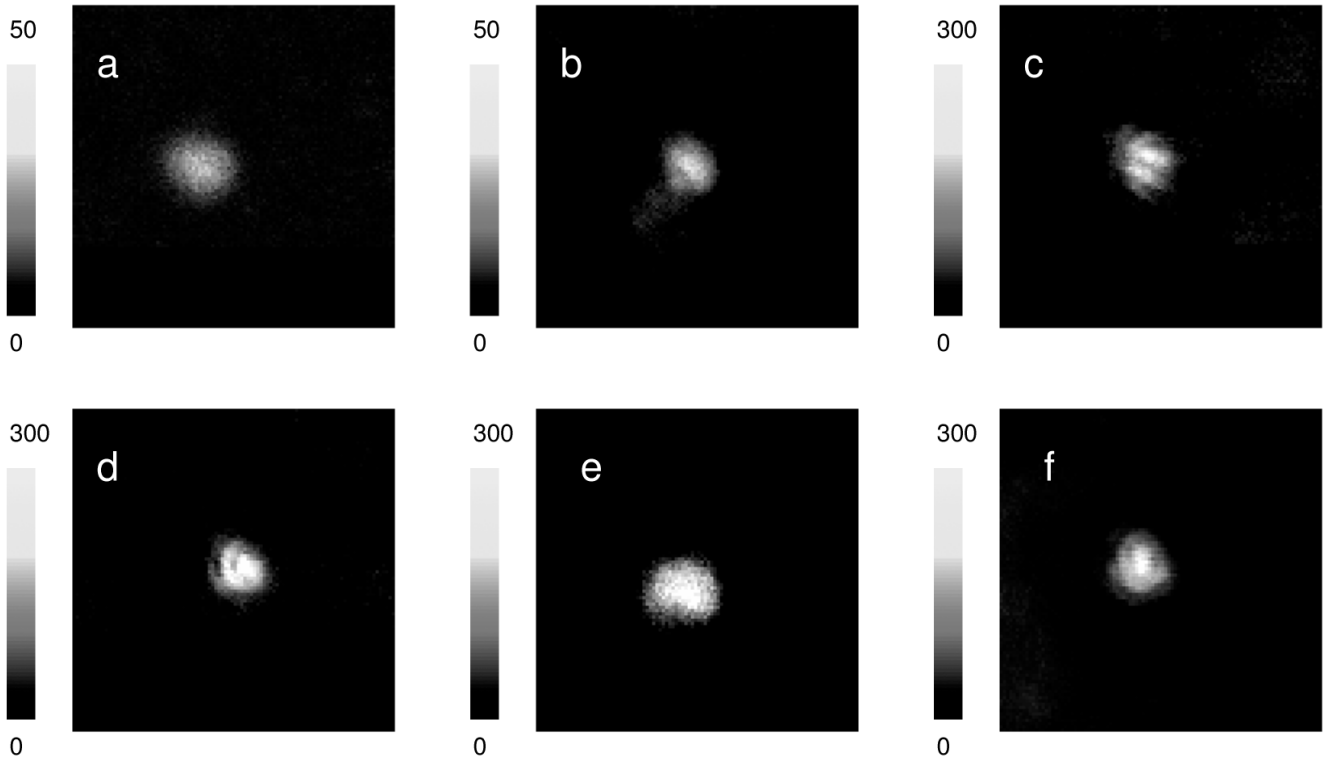

Figure 7.

Single nanoparticle luminescent images of (a) Eu(III)-encapsulated silica sphere with approx. 300 complexes in the absence of metal, (b), silica sphere seeded by 5 nm silver colloids, (c) 5 nm silver shell, (d) 20 nm silver shell, (e) 30 nm silver shell, and (f) 40 nm silver shell. Note that the scale bars are different. The 5 × 5 μm images are 100 × 100 pixels within integration time of 0.6 ms per pixel.

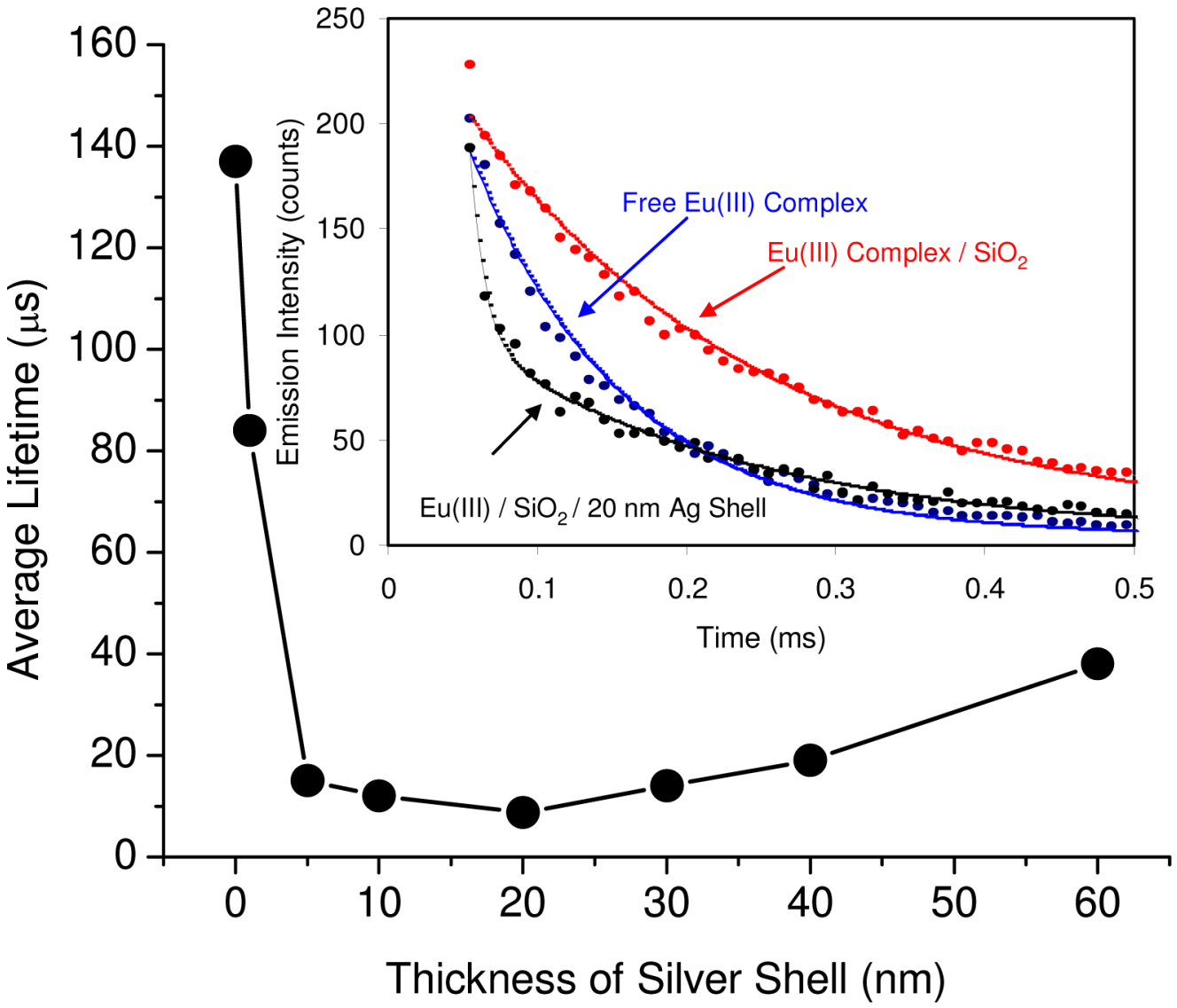

Figure 8.
Dependence of emission lifetime of Eu(III)-encapsulated silica core/silver shell structures on the silver thickness. The inset represents the emission decays of free Eu(III) complex, Eu(III)-encapsulated silica sphere in the absence of metal, and Eu(III)-encapsulated silver shell with 20 nm thickness upon excitation at 330 nm.

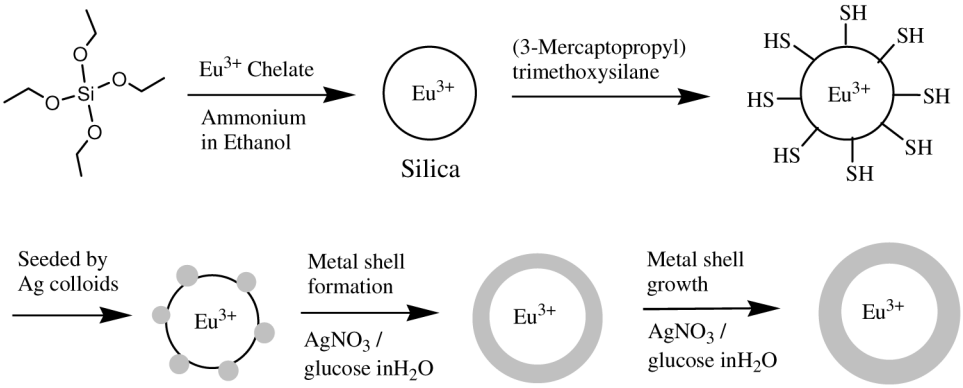

Scheme 1.
Construction of silver nanoshells on Eu(III)-encapsulated silica spheres in layer-by-layer growth model.

Table 1

Collection of emission lifetime for Eu(III) complex - encapsulated silica sphere and silver shells grown on the silica sphere.

Samples	τ_i (μs)	α_i	$<\tau>$ (μs)	χ_R^2
Free Eu(III) complex	39	0.71	75	1.3
	164	0.29		
Eu(III) complex in silica sphere	35	0.51	137	1.5
	243	0.49		
Ag seeded-silica sphere	15	0.67	84	1.1
	224	0.33		
5 nm silver shell	12	0.98	15	1.3
	212	0.02		
10 nm silver shell	11	0.99	12	1.6
	204	0.01		
20 nm silver shell	8	1.00	8.7	0.9
	213	0.00		
30 nm silver shell	11	0.787	14	1.0
	194	0.213		
40 nm silver shell	14	0.97	19	1.4
	228	0.03		
60 nm silver shell	21	0.92	38	1.2
	229	0.08		